

EXPERIMENTAL INVESTIGATION OF TURBINE BLADE-TIP EXCITATION FORCES

Manuel Martinez-Sanchez, Belgacem Jaroux, Seung Jin Song,
Soomyung Yoo, and Taras Palczynski
Massachusetts Institute of Technology
Cambridge, Massachusetts

51-37
12845
p-12

Abstract

This paper presents results of a program to investigate the magnitude and parametric variations of rotordynamic forces which arise in high power turbines due to blade-tip leakage effects.

Five different unshrouded turbine configurations and one configuration shrouded with a labyrinth seal were tested with static offsets of the turbine shaft. The forces along and perpendicular to the offset were measured directly with a rotating dynamometer. Exploration of casing pressure and flow velocity distributions was used to investigate the force-generating mechanisms. For unshrouded turbines, the cross-forces originate mainly from the classical Alford mechanism (nonuniform work extraction due to varying blade efficiency with tip gap) while the direct forces arise mainly from a slightly skewed pressure pattern.

The Alford coefficient for cross-force was found to vary between 2.4 and 4.0, while the similar direct force coefficient varied from 1.5 to 3.5. The cross-forces are found to increase substantially when the gap is reduced from 3.0% to 1.9% of blade height, probably due to viscous blade-tip effects. The forces also increase when the hub gap between stator and rotor decreases. The force coefficient decreases with operating flow coefficient.

In the case of the shrouded turbine, most of the forces arise from nonuniform seal pressures. This includes about 80% of the transverse forces. The rest appears to come from uneven work extraction (Alford mechanism). Their level is about 50% higher than in the unshrouded cases.

* This work was performed under Contract NAS 8-35018 from NASA, Marshall SFC, Glenn E. Wilmer, Jr., Technical Monitor.

Nomenclature

C_x, C_y, C_z	Fluid velocity components along x, y, z
C_θ	same as C_y
C_{ij}	Fluid Damping Matrix for turbine displacements
e, e_x	Turbine eccentricity
f, f_y	Tangential force per unit length
F_x	Net force on turbine in direction of offset
F_y	Net force on turbine perpendicular to offset
H	Blade height
K_{ij}	Fluid stiffness matrix for turbine displacements

PRECEDING PAGE BLANK NOT FILMED

K_0	Structural stiffness for turbine displacements
M	Rotor mass
P, P_t	Pressure, total pressure
Q	Turbine torque
R	Turbine mean radius
U	Turbine wheel speed (ωR)
x	Axial coordinate
y	Tangential coordinate
z	Radial coordinate
α_x	Force coefficient along offset (Eq. 8)
α_y	Force coefficient perpendicular to offset (Eq. 8)
β	Sensitivity of tangential force to relative gap, $\beta = -\frac{\partial f_y}{\partial(\delta/H)}$
β_η	Sensitivity of local efficiency to relative gap, $\beta = -\frac{\partial \eta}{\partial(\delta/H)}$
δ	Blade tip gap
ϕ	Flow coefficient, $C_x/\omega R$
ϕ_f, ϕ_p	Phase angles for fluid force (Eq. 10) and wall pressure (Eq. 13)
ρ	Fluid density
θ	Azimuth angle
ω	Angular frequency of turbine spin
Ω	Whirl angular frequency
ζ	Rotor damping factor

1. Introduction

The existing large body of literature on turbomachine tip leakage has been mainly motivated by the substantial contribution of these leakages to losses. H.J. Thomas (1), in 1958, and J.S. Alford (2), in 1964, independently pointed out that, in a turbine undergoing transverse vibrations (e.g. a whirling motion), the portion of the blading with the smaller tip gap would produce greater tangential driving force than its 180° opposite. Upon integration, this difference in work extraction results in a cross force tending to promote forward whirl, leading to rotordynamic instability.

Both Alford and Thomas showed that, if the tangential force f per unit length is assumed to vary linearly with the ratio δ/H of local tip gap to blade height

$$f = f_0 - \beta \frac{\delta}{H} \quad (1)$$

and if the shaft is offset instantaneously by e_x along the o_x direction, then a cross-force F_y equivalent to

$$F_y = \frac{\beta}{2} \frac{Q}{R} \frac{e_x}{H} \quad (2)$$

arises where Q is the turbine torque and R its mean radius. The factor β has become known in the U.S. as the Alford coefficient which is quoted as varying between 0 and 6. The German literature uses a factor called the "excitation coefficient", k_2 , which is equivalent to $\beta/2$. Implicit in the Alford/Thomas model is the assumption that the flow remains perfectly uniform up to the offset turbine, as well as downstream of it, so that only the local efficiency, as determined by the local tip gap, is of concern. Two of the consequences of these models are (a) the absence of a direct force component (in the offset direction, and (b) the absence of frequency dependence (no damping).

If only a cross-coupled coefficient (K_{xy}) is generated, it can be easily shown that the damping factor required for stabilization against it would be

$$\zeta_{\min} = \frac{1}{2} \frac{K_{xy}}{K_o} = \frac{\beta}{4} \frac{Q}{RH K_o} \quad (3)$$

This can be very substantial in high-pressure turbines. For the SSME H₂ turbopump, $Q = 12800 \text{ Nm}$, $R = 0.129\text{m}$, $H = 0.023\text{m}$, and $K_o = MR \Omega T$ $\Omega_o^2 = 1.9 \times 10^8 \text{ Nm}$, giving $\zeta_{\min} = 0.019$, or a log decrement of 12%.

Relatively little work on these forces has been done since the pioneering efforts of Alford and Thomas. Thomas' collaborators at the T.U. Munich produced the most detailed experimental data. Ulrichs (3) used a relatively low power facility, with blade Reynolds numbers below 10^5 , and measured cross-forces mainly on shrouded turbines, although one unshrouded case was also tested. He identified the shroud seal as the major contributor to the cross-forces. The mechanics of these seal-related forces has been more clearly elucidated since (see for instance Refs. (4), (5), (6)), and is distinct from the uneven work extraction of Alford-Thomas effect. In his unshrouded tests, Ulrichs noted a cross-force reduction with increasing mean tip gap, and an increase with axial stator-rotor spacing. The measured forces were roughly compatible with the simple Alford argument. Wohlrab (7), used a larger, pressurized air turbine, capable of stator leaving Reynolds numbers up to 5×10^5 , but tested only shrouded turbines. Strong non-linearity of force vs. displacement was noted in the cases with smaller forces, which raises questions about accuracy. Limited dynamic testing was accomplished as well. As in Ref. (3), the main mechanism in these tests was through seal pressure effects, rather than through uneven work extraction. Vance and Laudadio (8), did some very low power tests on a fan with statically moveable casing, and reported measured cross-forces, but no aerodynamic data. Ehrich (9) has recently inferred Alford forces from compressor efficiency test data, and argues that these forces become backward-whirling at pressure ratios above the normal operating point.

We have performed extensive force measurements on an unshrouded turbine identical to the first stage of the Shuttle LH turbopump, and also on a shrouded derivative of it. These were supplemented by flow field measurements and theoretical analysis to clarify mechanisms. In this paper, we will describe the test facility (Sec. 2), and present the force and flow data (Sec. 3-6).

2. Experimental Apparatus

The test facility is a pressurized closed loop, filled with Freon 12 gas, and equipped with a gas blower, heat exchanger/cooler, removable test section, power extraction generator and data acquisition system. Nominal operating conditions are 2.0 atm mean pressure and 4.5 Kg/sec flow rate. Flow rate is mainly controlled by a manual series valve, with help from a bypass valve at low flow. Speed is controlled through generator excitation control.

The test section area is shown in Fig. 1. The upper section (12) of the casing can be rotated and carries the stator and the hub, as well as a variety of flow probes. The turbine shaft connects to the turbine via a four-post rotating dynamometer (14), and is supported by two bearings. The bearings are carried in a heavy cylindrical structure which can be translated sideways by means of four stiff rods, two on each side. Static offsets are achieved (to an accuracy of ± 0.5 mil) by insertion or removal of calibrated shims (11). The dynamometer can sense all components of force and torque on the turbine, and the signals from its 9 strain gauge bridges are carried through the shaft to the slip-ring assembly (23). These signals were sampled 32 or 64 times per revolution, on a pattern which was phase-locked to the rotor by means of signals from an auxiliary encoder (18). The data were ensemble-averaged over 128 or 256 revolutions, to reduce low-frequency noise, and were then numerically projected on fixed axes to extract the DC forces of interest (F_x along the displacement axis, F_y perpendicular to it). Despite sizable second harmonic contamination from the flex joints in the shaft, these DC components were extracted with an accuracy and repeatability of $\pm 0.05 \ell b_f$ (the forces F_x and F_y ranged to a few ℓb_f).

The characteristics and design parameters of the unshrouded test turbine are summarized in Table 1. Due to the low pressure ratio, compressibility effects are minimal, and similarity would be ensured by matching flow and work coefficients, and Reynolds number. The first two are indeed matched to the SSME LH turbine. The Reynolds number (based on stator exit velocity and blade height) is 1.4×10^6 , compared to 5.6×10^6 in the SSME turbine; since both are well above transition (10^5 - 2×10^5) no significant difference is expected. A limited test of this insensitivity was provided by comparison runs at 1 atm and 2 atm loop pressure, in which no difference was detected in the nondimensional cross-force characteristics.

After the unshrouded turbine tests, the same turbine was modified by removing the outer 6.49 mm (out of a blade height of 22.9 mm) and installing a continuous shroud band with a 2-ridge labyrinth seal (as shown in Fig. 2). Due to the partial flow blockage of the unrecessed seal, the optimum flow rate at the design speed of 3440 rpm dropped to 3.16 Kg/sec, the optimum efficiency dropped to 74%, and the corresponding pressure ratio was reduced to 1.14.

The test matrix is summarized in Table 2, with the geometrical notation contained in Fig. 3.

3. Force Data for the Unshrouded Turbine

Typical force vs. displacement plots are shown in Fig. 4, which corresponds to Configuration 1 of Table 2, at its design condition. The plots for Configurations 2-5 are qualitatively similar. In these graphs, the negative F_x slope indicates a restoring direct force, while the positive F_y slope indicates a forward-whirling cross-force. Each test was repeated three times, and all test results are shown to illustrate the degree of repeatability of the data. The fact that the forces are not exactly zero at zero eccentricity is due to a combination of casing out-of-roundness and positioning error. Despite the relatively large offsets (± 15 mil on a mean gap of 27 mil), the F_y data show no departure from linearity. By contrast, the F_x data show in all cases a slight s-shaped curvature, with the slope increasing with eccentricity.

As noted in the Introduction, the simple Alford theory would predict $F_x = 0$. However, the data show $|F_x|$ of the same order as $|F_y|$, and a different mechanism, or a variation on Alford's postulated mechanism, must be involved.

The results of the measurements for all configurations are reported in nondimensional form in Table 3. The coefficients α_x and α_y are obvious generalizations of Alford's b:

$$\alpha_x = \frac{2F_x R}{Q(e/H)} ; \quad \alpha_y = \frac{2F_y R}{Q(e/H)} \quad (4)$$

where the notation has been changed from b , which is strictly the sensitivity of blade tangential forces to tip gap, to a , which is a measure of the cross-forces, and may or may not be equal to b (indeed, there is no b counterpart to α_x). The forces at $e=0$ have been subtracted from F_x and F_y in calculating α_x and α_y .

Table 3 indicates a general increase of α_y with speed at a fixed flow rate, or a decrease with the flow coefficient $\phi = C_x/(wR)$. This is displayed in Fig. 5. The theoretical curve shown is from an xz actuator disk theory which will not be discussed in this paper (see Ref. 10).

A second trend in the data is a substantial increase of the force coefficient (both $|\alpha_x|$ and α_y) as the mean radial gap is reduced. This can be seen by comparing Configurations 2 (gap 3% of blade height) and 4 (gap 1.9%), both with the widest axial hub gap d' , and also by comparison of Configurations 3 and 5, similarly related, but with a narrower axial hub gap. Averaging over the various speeds, the effect amounts to a 0.6 decrease in α_y (19%) per 1% increase in $\bar{\delta}/H$ (wide axial gap), or a 0.7 (21%) per 1% for the narrow axial gap. Of course, since only two gap values were tested, there is no confirmation of the linearity of this effect. The theory (Ref. 10) predicts a much smaller effect of $\bar{\delta}$ on α_y , and there are some indications from the flow data (Sec. 4) that viscous flow effects in the narrow tip flow passages may be responsible. This trend had been previously reported by Urlichs (3) as well.

Configurations 2 and 3 differ only in the hub axial gap d' , while Configuration 1 differs from 2 and 3 in both, d' , and the stator-to-rotor blade spacing, d . All three configurations have $\bar{\delta}/H = 3\%$. Thus, if we postulate a linear variation of α_y with d and d' , the data in Table 3 can be used to extract the separate sensitivities of α_y to these gap values. Similarly, comparison of Configurations 4 and 5 can yield the d' sensitivity for the cases with a narrow radial tip gap. The results (Table 4) are inconclusive for d , but are unambiguous as to sign and general magnitude for the hub gap d' . We have not been able so far to find a satisfactory explanation for this effect. Opening the gap d' should have the direct effect of reducing the pressure non-uniformity in the stator-rotor space, and to the extent that this nonuniformity contributes to the cross-force (see Sec. 4), this would indeed reduce α_y . On the other hand, these pressure nonuniformities also redistribute the upstream flow in a manner which tends to dampen the Alford effect, as our x - y actuator disk analysis (Ref. 10) makes clear. The net result must then depend on the balance of these two effects. A more complete analysis of the flow data, and additional theoretical development are needed in this area. Urlichs (3) found the opposite trend (α_y increasing with axial gap), but his geometry was such that both d and d' were varied simultaneously.

In addition to the direct force measurements, both upstream and downstream flow fields were explored through a set of static wall pressure taps and directional probes. More details about this instrumentation and flow data can be found in Ref. 10. The surveys upstream of the stator indicated very small departures from tangential uniformity. On the other hand, the wall pressure surveys downstream of the stator do show a well-resolved nonuniformity. Fig. 6 shows the pressure pattern for the inter-blade row region and the rotor blade tip region. For the region between stator and rotor a pressure fluctuation amplitude of about $0.0027P_{10} = 0.22 \rho C_{x0}^2 / 2 = 0.028 \rho (\omega R)^2$ for $e/H =$

0.019. The pressure minimum is about 25° ahead of the maximum gap location. The pressure nonuniformity increases in amplitude as one moves downstream over the rotor blades, particularly in their narrow-gap sectors, but it then returns downstream to the same level as between rotor and stator. Thus, the turbine eccentricity is felt upstream and downstream of it, through potential effects, with a length scale of the radius R, and, from limited probing data, spanning the passage depth as well.

At 3 chord lengths downstream of the turbine, the velocity data were obtained to a depth of 75% span, using a 3 hole probe. The tangential distribution is shown in Figure 7, where the mean (centered turbine) tangential velocity has been subtracted out. Based on consistency among various probes and also with the dynamometer data, the errors appear to be under 10%. The positive tangential velocity values seen near the bigger gap region (180°) indicate underturning by the rotor blades. The magnitude seems to be uniform in the outer 5% of the span, gradually decreasing towards the hub.

Thus, two main sources of lateral force on the turbine due to the flow properties can be identified: 1) a tangentially non-uniform flow turning which leads to uneven work extraction; and 2) a non-uniform static pressure distribution acting on the turbine hub. Both forces can be integrated around the perimeter to a direct force and a cross force. Integration of the pressure nonuniformity is straightforward. We assumed the pressure acting on the hub is that observed before and after the rotor, since the excess nonuniformity over the rotor blades appears to be a near-tip effect. For the work-defect forces, we used the Euler turbine equation locally to calculate an azimuth-dependent tangential force per unit length

$$f_y = \int_0^H \rho C_x \Delta C_y dr \quad (5)$$

where C_x is taken to be the mean axial velocity, and the flow turning ΔC_y is from our velocity surveys.

The results for Configurations 4 and 5 are shown in Table 5, where we report the separate pressure and work-defect contributions to a_x and a_y , their sum, and for reference, the dynamometer-measured data. Similar results were also obtained (for all configurations) using velocity data at 1.5 chords downstream of the rotor (Ref. 10). Most of the direct force is due to the pressure force while the cross force is caused by both the pressure force and the blade force. The cross force coefficients, a_y , are larger than expected for this low-reaction turbine on the basis of work-defect arguments. Clearly, the pressure component, not previously identified, is an important factor.

All of the data reported here are for static offsets. An attempt at measuring cross forces under dynamic conditions (using an inertial shaker) was unsuccessful due to excessive vibratory noise. The simple theory of Alford predicts zero damping, while a more complete model (Ref. 10) indicates significant damping due to lag in tangential flow redistribution. Given the large magnitude of the statically measured forces, measurements under dynamic conditions should be undertaken in order to complete our understanding of Alford forces.

4. Forces in a Shrouded Turbine

The turbine was modified, as described in Section 2 of this paper, for the shrouded case, and dynamometer and flow data were obtained. As in the unshrouded cases, the forces scale linearly with eccentricity, and a sinusoidal pressure pattern with a large amplitude develops over the shroud band. Table 6 shows the excitation coefficients from the dynamometer data, and the pressure data at the design speed. Compared to the unshrouded cases, the excitation coefficients are larger by a factor ranging from 1.5 to 2.0.

The nonuniform pressure distribution produces both direct and cross forces which are smaller than those measured with the dynamometer. For this configuration, no measurements were taken of the velocity perturbations, because, due to the presence of the unrecessed shroud, the flow was very turbulent downstream of the rotor. If it is assumed that the work defect mechanism contributes primarily to the cross force as in the unshrouded cases, the discrepancy in the direct force excitation coefficient cannot be explained. Furthermore, the small difference in the cross force excitation coefficients for the shrouded case suggests that the pressure effect, instead of the work defect effect, is primarily responsible for the cross force. Lastly, the pressure non-uniformity, which can be detected upstream and downstream of the shroud, shows again a flow redistribution on the scale of the turbine radius.

A linear labyrinth seal model based on the work of Millsaps (6) was extended to include the effects of non-uniformities in the flow both upstream and downstream of the shroud and was used to analyze the shrouded data. It was found that the non-uniformities have a large effect on the model's predictions, essentially doubling the magnitude of both the direct and the cross force, but even after this correction, the model underpredicts the forces by about 40%. No complete theory exists of a seal interacting with the flow field of the turbine blading. Palczynski (11) discusses, in greater detail, the work on the shrouded turbine.

8. Conclusions

This work has confirmed the existence of the destabilizing forces suggested by Thomas and Alford. The general scaling and order of magnitude are also consistent with their insights. However, some new effects in the unshrouded cases include the following:

- 1) In addition to a non-uniform work extraction, a non-uniform pressure distribution also exists.
- 2) The forces increase significantly as the mean tip gap is reduced, confirming an earlier result.

The lateral forces in shrouded turbines can be larger than those in unshrouded turbines. This is due to a large nonuniformity in the seal gland pressure, which now dominates over the work defect contribution.

Alford force measurements under dynamic conditions are recommended in order to investigate the possible existence and magnitude of a damping component of this force.

References

- (1) Thomas, H.J., "Instabile Eigenschwingungen von Turbinenlaufem Angefacht durch die Spaltstroemung in Stopfubuchsen und Bechauchflug (Unstable Natural Vibrations of Turbine Rotors Induced by the Clearance Flows in Glands and Blading)", Bull. de L.A.I.M. 71 NO 11/12, 1958, PP. 1039-1063.
- (2) Alford, J.S., "Protecting Turbomachinery from Self-Excited Rotor Whirl", Journal of Engineering for Power, October 1965, pp. 333-334.
- (3) Urlichs, K., "Clearance Flow Generated Transverse Forces at the Rotors of Thermal Turbomachines", NASA TM-77292, Translation of Ph.D. Dissertation, Munich Technical University, 1975.

- (4) Iwatsubo, T., "Evaluation of Instability Forces of Labyrinth Seals in Turbines or Compressors", NASA CP-2133, 1980, PP. 139-169.
- (5) Scharrer, J.K., Childs, D.W., "Theory Versus Experiment for the Rotordynamic Coefficients of Labyrinth Gas Seals: Parts 1 & 2", ASME Journal of Vibration, Acoustics, Stress and Reliability in Design, Vol 110., No. 3, 1989, pp. 270-287.
- (6) Millsaps Jr., K.T., "The Impact of Unsteady Swirling Flow in a Single Gland Labyrinth Seal on Rotordynamic Stability: Theory and Experiment", Ph.D. Thesis, Department of Aeronautics and Astronautics, M.I.T., 1992.
- (7) Wohlrab, R., "Experimental Determination of Gap Flow Conditioned Forces at the Rotors of Thermal Turbomachines", NASA TM-77293, Translation of Ph.D. Dissertation, Munich Technical University, 1975.
- (8) Vance, J.M., and Laudadio, F.J., "Experimental Measurement of Alford's Force in Axial Flow Turbomachinery", ASME Paper 84-GT-140, June 1984.
- (9) Ehrich, F., Unpublished Report, 1992.
- (10) Martinez-Sanchez, M., and Jaroux, B., "Turbine Blade Tip and Seal Clearance Excitation Forces", Phase III Report on NASA Contract No. NAS8-35018, May, 1992.
- (11) Palczynshki, T.A., "Experimental and Theoretical Investigation of Rotordynamic Instability in a Shrouded Turbine", S.M. Thesis, Department of Aeronautics and Astronautics, M.I.T., 1992.

Table 1
Design Parameters for SSME Fuel Turbopump First Stage
and the Test Facility Turbine

Parameter	SSME Fuel Turbopump First Stage	Test Facility Turbine
Flow coefficient, ϕ	0.58	0.58
Work coefficient, Ψ	1.508	1.508
Stator exit angle	70°	-
Relative rotor inlet angle	43.9°	-
Rotor exit angle	60°	-60°
Absolute exit angle	-3.1°	-3°
Degree of reaction	0.216	0.216
Rotor mean radius, cm (in)	12.88 (5.07)	12.88 (5.07)
Number of rotor blades	63	63
Rotor blade height, cm (in)	2.17 (0.854)	2.17 (0.854)
Rotor blade chord, cm (in)	2.21 (0.870)	2.21 (0.870)
Rotation Rate, rpm	34,560	3440
Axial flow velocity, m/s (in/s)	262 (10,300)	26 (1020)
Mass flow rate, kg/s (slug/s)	71.8 (4.92)	4.48 (0.307)
Inlet pressure, kPa (psi)	34,950 (5069)	224 (32.43)
Inlet temperature	1053 (1436)	300 (80)
Pressure ratio	1.192	1.231
Efficiency	0.821	0.80

Table 2 The Test Matrix

Conf #	t_m/H (%)	d/c (%)	d'/c (%)	Shroud (Y/N)	m/m_{dcs} (%)	ω/ω_{dcs} (%)	c/t_m Range (%)
1	3.0	50	38	N	50	100	± 67 ($e = \pm 0.46$ mm)
					100	70	
					100	100	
					100	110	
					100	70	
					100	100	
					100	110	
2	3.0	26	15	N	100	70	± 67
						100	
						110	
3	3.0	26	1.3	N	100	70	± 67
						100	
						110	
4	1.9	26	15	N	100	70	± 59 ($e = \pm 0.25$ mm)
						100	
						110	
5	1.9	26	1.3	N	100	70	± 59
						100	
						110	
6	4.5	26	1.3	Y	100	70	± 59
						100	
						110	

Table 3
Nondimensional Force Coefficients from Dynamometer

Configuration	ω / ω_{design}	α_x	α_y
1	0.7	-2.12	2.43
1	1.0	-2.81	2.57
1	1.1	-3.42	3.66
2	0.7	-1.54	2.49
2	1.0	-2.14	2.96
2	1.1	-2.46	3.23
3	0.7	-1.47	2.87
3	1.0	-1.87	3.02
3	1.1	-2.04	3.43
4	0.7	-2.93	3.38
4	1.0	-3.42	3.55
4	1.1	-3.65	3.72
5	0.7	-2.82	3.83
5	1.0	-3.47	3.98
5	1.1	-3.50	4.04

Table 4
Sensitivity of Cross-Force to Axial Stator-Rotor Spacing (d) and Hub Axial Gap (d')
(See Figure 6 for definitions)

$\bar{\delta} / H$	ω / ω_{des}	$\partial\alpha_y / \partial(d/c)$	$\partial\alpha_y / \partial(d'/c)$
0.030	0.7	2.42	-2.78
0.030	1.0	-1.21	-0.44
0.030	1.1	-1.00	-1.44
0.019	0.7	-	-3.32
0.019	1.0	-	-3.13
0.019	1.1	-	-2.37

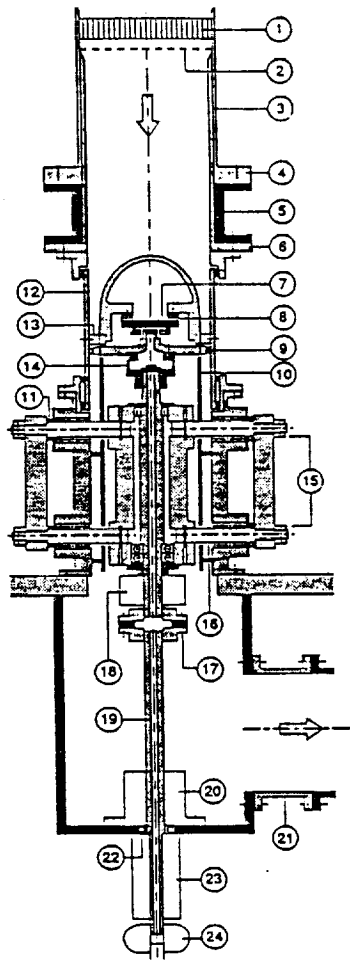
Table 5 Contributions from work defect (wd) and pressure (p) to the force coefficients α_x , α_y at design conditions, and comparison to dynamometer data.

Configuration	$(\alpha_x)_{wd}$	$(\alpha_x)_p$	$(\alpha_x)_{total}$	$(\alpha_x)_{dyn}$
4	-.6	-2.6	-3.2	-3.36
5	-.6	-2.3	-2.9	-3.47

Configuration	$(\alpha_y)_{wd}$	$(\alpha_y)_p$	$(\alpha_y)_{total}$	$(\alpha_y)_{dyn}$
4	2.1	1.6	3.7	3.55
5	1.9	2.2	4.1	3.98

Table 6 Nondimensional force coefficients from the dynamometer and pressure data for the shrouded turbine

Configuration	ω / ω_{design}	α_x	$(\alpha_x)_p$	α_y	$(\alpha_y)_p$
6	0.7	-4.06		5.94	
6	1.0	-5.63	-3.8	6.28	6.0
6	1.1	-6.00		6.37	



- (1) Flow straightener
- (2) Screen
- (3) Main loop piping
- (4) Flange
- (5) Flexible insert
- (6) Liner
- (7) Snubber bearing
- (8) Snubber support
- (9) Test turbine
- (10) Flow-smoothing shield
- (11) Shims
- (12) Rotatable casing
- (13) Stator blades
- (14) Rotating dynamometer
- (15) Bolts to secure shaft
- (16) Turbine-offsetting rods
- (17) Upper flex joint
- (18) Optical encoder
- (19) Intermediate shaft
- (20) Double-acting seal
- (21) Flexible insert
- (22) Pivoting bearing
- (23) Slip ring assembly
- (24) Lower flex joint

Figure 1: Schematic of the turbine test section.

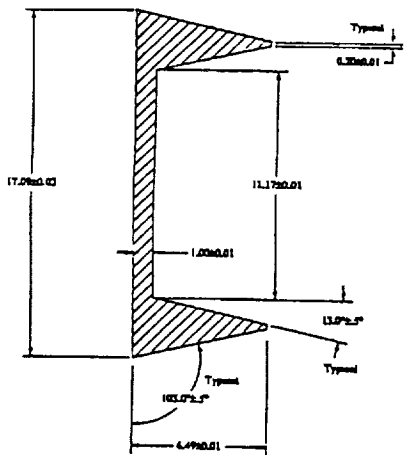


Figure 2: Shroud-seal for turbine. Dimensions in mm.

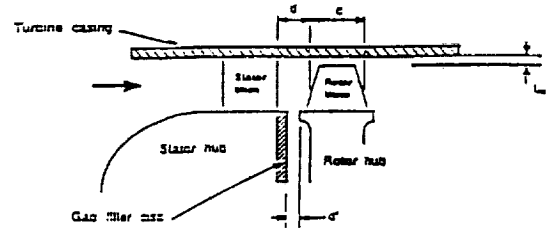


Figure 3: Schematic of turbine's major dimensions of interest.

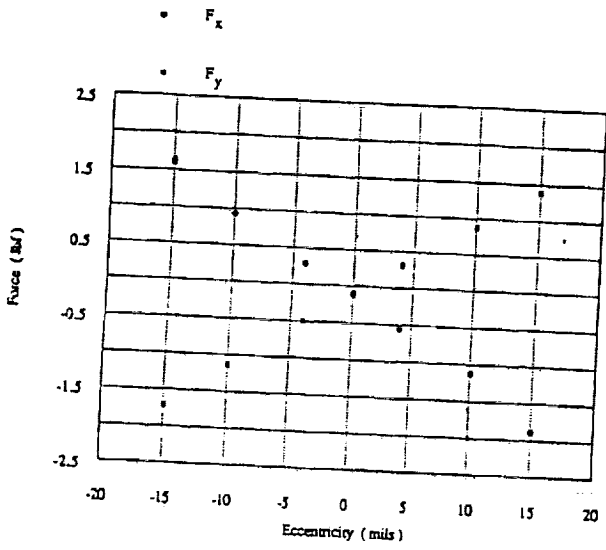


Figure 4: F_x and F_y versus e
(Conf. 1, $\omega/\omega_0 = 1.0$).

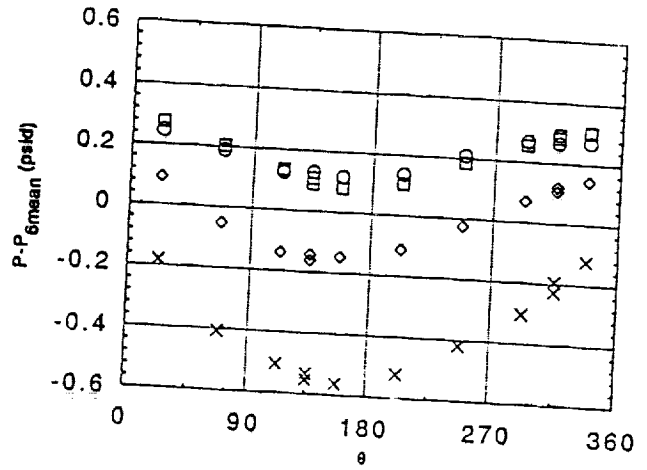


Figure 6: Wall tap pressure between stator and rotor(4) and over the rotor blade tip(5,6, & 7)
(Conf. 1, $e/H = 0.019$).

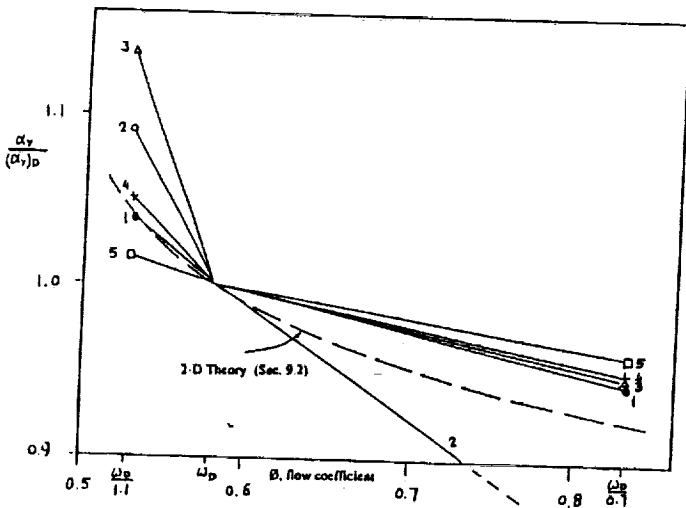


Figure 5: Effect of f on α_y
(Conf. 1, $e/H = 0.019$).

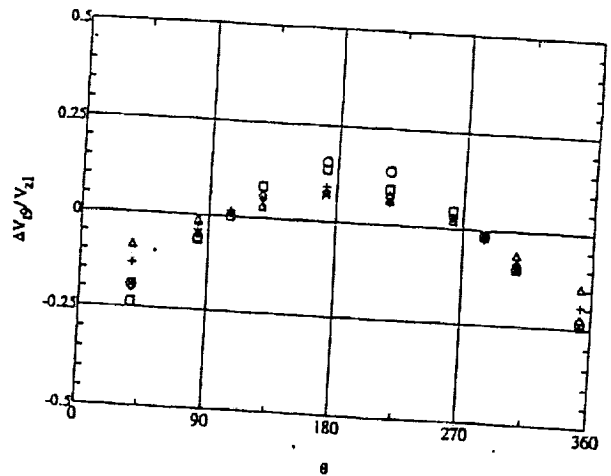


Figure 7: Tangential velocity at station 9
(Conf. 4, $e/H = 0.019$).